Electronic Supplementary Material (ESI) for Journal of Materials Chemistry A.

Supporting information

Porous Zn cathode for Li-CO_2 battery generating fuel-gas CO

Jiafang Xie, Qin Liu, Yiyin Huang, Maoxiang Wu, and Yaobing Wang*

CAS Key Laboratory of Design and Assembly of Functional Nanostructures, and Fujian Provincial Key Laboratory of Nanomaterials, State Key Laboratory of Structural Chemistry, Key Laboratory of Optoelectronic Materials Chemistry and Physics, Fujian Institute of Research on the Structure of Matter, Chinese Academy of Sciences, Fuzhou, Fujian 350002, China.

*To whom correspondence should be addressed: wangyb@fjirsm.ac.cn

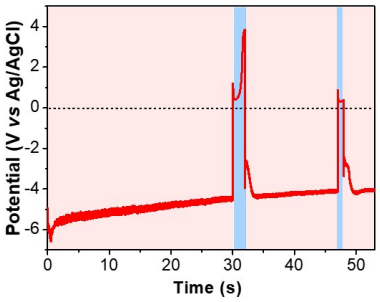

Figure S1. A typical potential *vs* time curve of redox-coupled electrodeposition for PF-Zn.

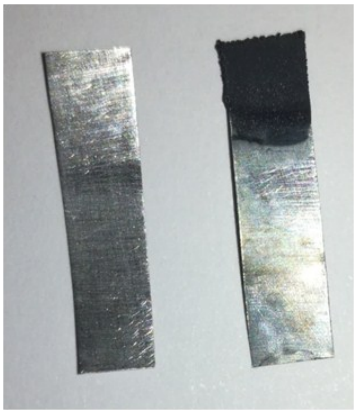

Figure S2. Typical photo of Zn foil before (left) and after (right) electrodeposition.

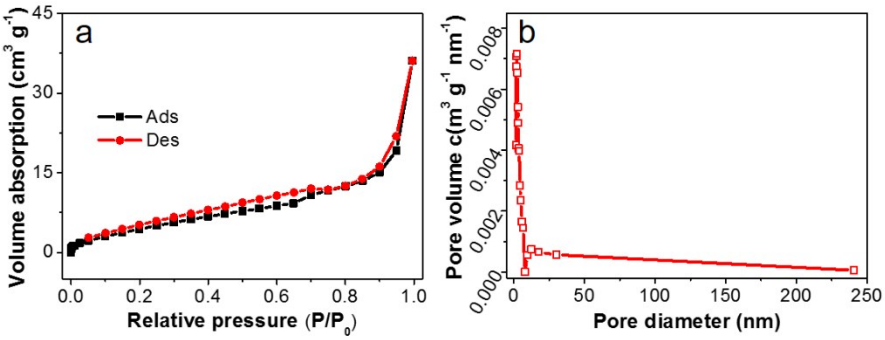

Figure S3. The N_2 adsorption-desorption isotherm and pore size distribution of PF-Zn. (a) The N_2 adsorption-desorption isotherm. (b) The pore size distribution.

PF-Zn possessed a specific surface area of 19.1 $m^2 g^{-1}$ and three characters in isotherm curve: 1) sharply increased absorbed volume over 0.8 P/P_0 indicated the macro pores, 2) the hysteresis loop from 0.1 P/P_0 to 0.8 P/P_0 indicated the meso pores, 3) sharply increased absorbed volume around 0.05 P/P_0 indicated the micro pores. These three kinds of pores were also suggested by the pore size distribution curve and PF-Zn exhibited a total pore volume of 0.062 $cm^3 g^{-1}$.

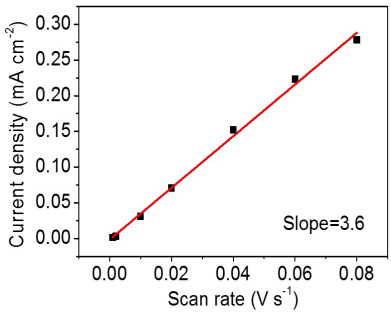

Figure S4. Double layer capacitance analysis of bare Zn foil substrate.

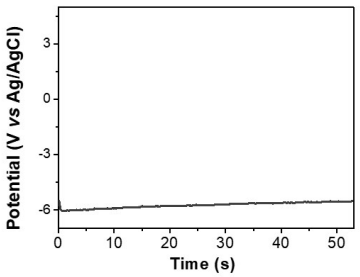

Figure S5. A typical potential *vs* time curve of constant cathodic current density deposition for porous Zn (P-Zn).

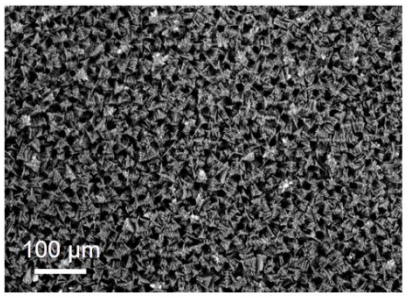

Figure S6. SEM image of P-Zn.

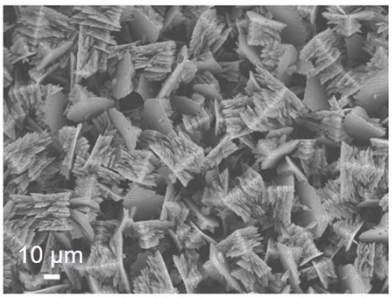

Figure S7. SEM image of P-Zn with higher magnification.

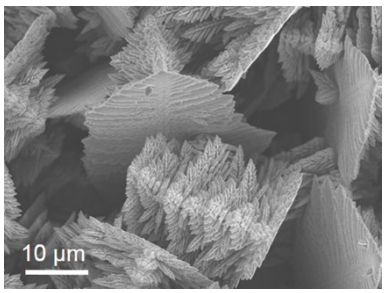

Figure S8. SEM image of P-Zn with further higher magnification.

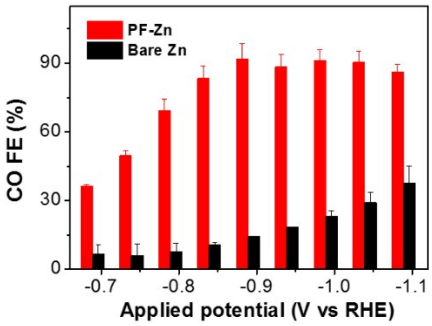

Figure S9. Electrochemical CO_2-to-CO electrochemical evaluation on PF-Zn in 0.1 M $KHCO_3$ with error bar.

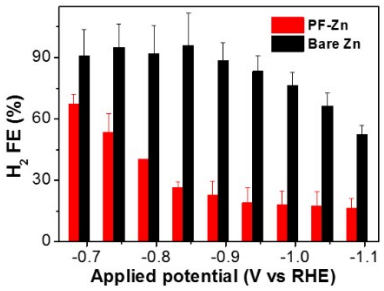

Figure S10. Electrochemical hydrogen evolution during CO_2-to-CO electrochemical evaluation on PF-Zn in 0.1 M $KHCO_3$ with error bar.

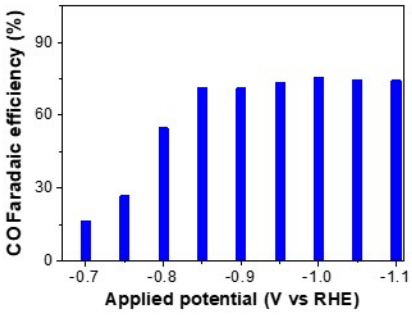

Figure S11. Electrochemical CO_2-to-CO electrochemical evaluation on P-Zn in 0.1 M $KHCO_3$.

Table S1. Reported Zn catalysts for electrochemical CO_2 reduction

Catalyst	Electrolyte	Max CO FE (overpotential)	Tafel slope	Reference
PF-Zn	**0.1 M $KHCO_3$**	**94% (780 mV)**	**181 mV dec^{-1}**	**This work**
P-Zn	0.1 M $KHCO_3$	75% (880 mV)	209 mV dec^{-1}	This work
h-Zn	0.5 M $KHCO_3$	85.4% (840 mV)	NM	*Angew. Chem. Int. Ed.*[1]
LiET-Zn	0.1 M $KHCO_3$	71% (690 mV)	149 mV dec^{-1}	*ACS Nano*[2]
Reduced nanoporous ZnO	0.25 M K_2SO_4	92% (1100 mV)	221 mV dec^{-1}	*Electrochem. Commun.*[3]
Zn dendrites	0.1 M $KHCO_3$	79% (990 mV)	260 mV dec^{-1}	*ACS Catal.*[4]
Bi	$[EMIM]BF_4$	95% (165 mV)	139 mV dec^{-1}	*J. Am. Chem. Soc.*[5]
Cu_4Bi	0.5 M $NaHCO_3$	~85% (590 mV)	NM	*Angew. Chem. Int. Ed.*[6]
Porous hollow fibre copper	0.3 M $KHCO_3$	72% (290 mV)	93 mV dec^{-1}	*Nat. Commun.*[7]
Oxided-derived Ag	0.1 M $KHCO_3$	80% (490 mV)	77 mV dec^{-1}	*Angew. Chem. Int. Ed.*[8]
MoSeS monolayers	$EMIMBF_4$:H_2O=4: 96(mol)	45% (940 mV)	NM	*Angew. Chem. Int. Ed.*[9]
Co_3O_4-CDots-C_3N_4	0.5 M $KHCO_3$	89% (490 mV)	NM	*Nat. Commun.*[10]

Notes: NM: not mentioned.

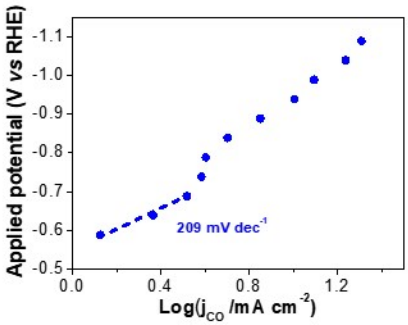

Figure S12. Tafel analysis about CO_2-to-CO electrochemical evaluation on P-Zn in 0.1 M $KHCO_3$.

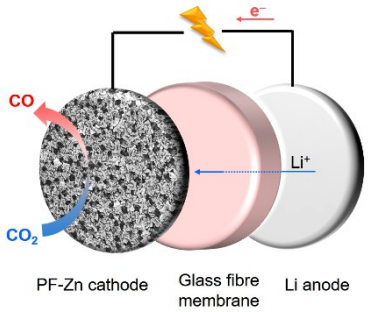

Figure S13. Schematic of the Li-CO_2 battery with PF-Zn cathode. The electrolyte: TEGDME and 1 M LiTFSI.

Figure S14. Photo of cathodic shell of coin-type cell used in the Li-CO_2 battery test.

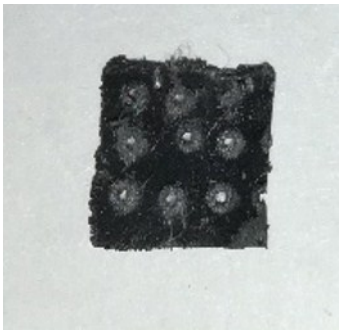

Figure S15. Photo of PF-Zn used in battery test.

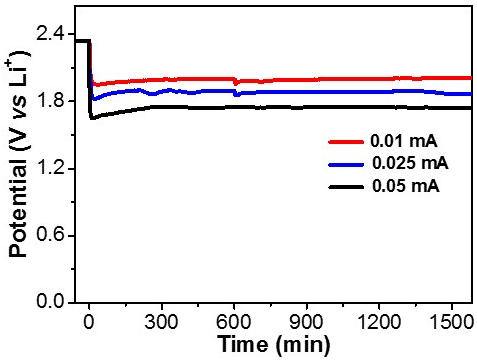

Figure S16. Galvanostatic discharge potentials of Li-CO_2 batteries with PF-Zn cathodes under several currents.

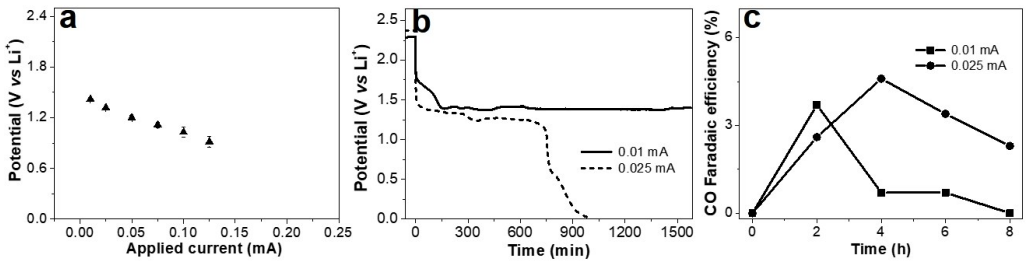

Figure S17. Galvanostatic discharge of Li-CO_2 batteries with bare Zn cathodes. (a) Discharge potentials profiles. (b) Discharge potential variation at long-term tests. (c) Max CO FE at several-currents during 10-h discharge.

The smaller CO generation with lower FE during Li-CO_2 batteries discharge (Fig. 4, S17, and S18) than during electrochemical evaluation (Fig. 3) was observed in both PF-Zn and bare Zn cathodes. This lower selectivity of CO generation from Li-CO_2 battery ($2Li^+ + 2CO_2 \rightarrow Li_2CO_3 + CO$) may be owing to the slow kinetics resulted from Li_2CO_3 forming and depositing on catalyst surface.

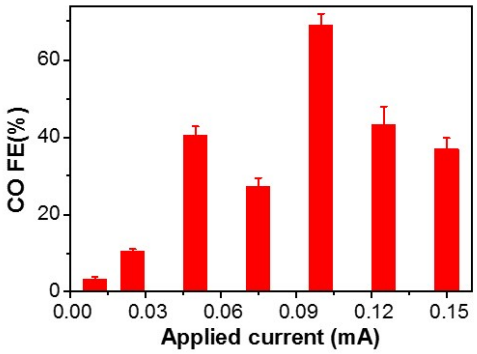

Figure S18. Max CO FE from Li-CO_2 batteries with PF-Zn cathodes at several currents during 10-h discharge with error bar.

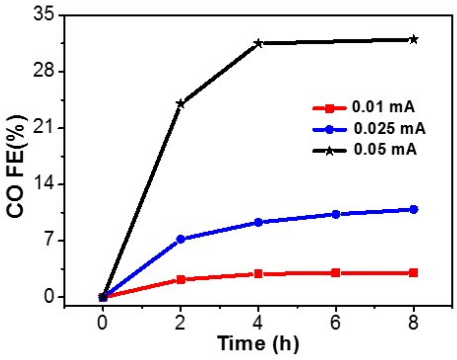

Figure S19. Max CO FE from Li-CO_2 batteries with PF-Zn cathodes at several currents during 10-h discharge.

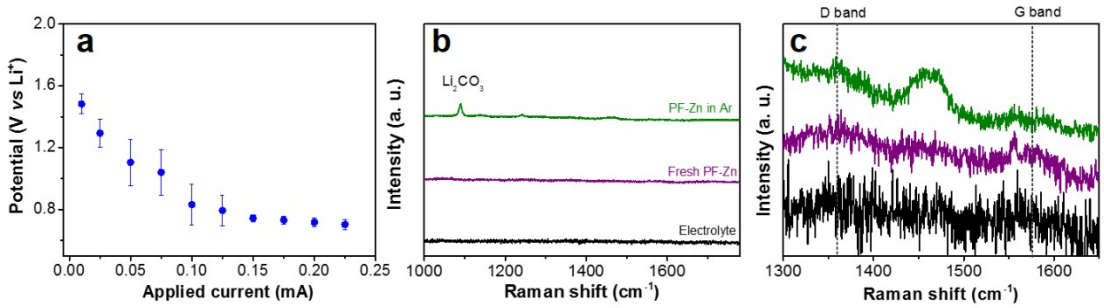

Figure S20. Galvanostatic discharge test of batteries with PF-Zn cathodes in Ar. (a) Discharge potentials profiles. (b) Raman spectra of PF-Zn after discharge tests. (c) High-resolution Raman spectra of PF-Zn in (b).

The control experiment with Ar supply instead of CO_2 filled cell was carried out, and the results revealed that 1) the discharge voltages were much lower than in CO_2, 2) no carbon-contained gas products (such as CO, CH_4, and C_2H_4) were detected, 3) H_2 was identified as the only gas product, 4) Li_2CO_3 and C were detected on the PF-Zn after the battery discharge in Ar. Based on above experiments, the electrolyte is possibly decomposed in our case, but the decomposition products do not contain CO. So CO generation from Li-CO_2 battery with PF-Zn cathode originated, most likely, from CO_2 reduction.

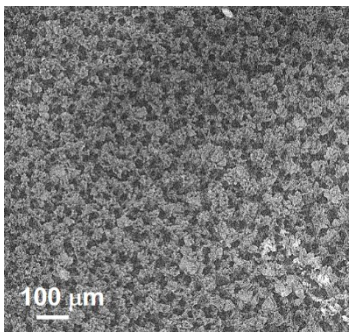

Figure S21. SEM image of PF-Zn cathode after battery discharge.

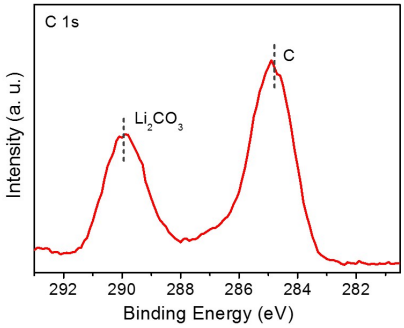

Figure S22. XPS spectrum of C 1s for PF-Zn after battery discharge.

References

1. D. H. Won, H. Shin, J. Koh, J. Chung, H. S. Lee, H. Kim and S. I. Woo, *Angew. Chem. Int. Ed.*, 2016, **55**, 9297-9300.
2. K. Jiang, H. Wang, W. B. Cai and H. Wang, *ACS nano*, 2017, **11**, 6451-6458.
3. X. Jiang, F. Cai, D. Gao, J. Dong, S. Miao, G. Wang and X. Bao, *Electrochem. Commun.*, 2016, **68**, 67-70.
4. J. Rosen, G. S. Hutchings, Q. Lu, R. V. Forest, A. Moore and F. Jiao, *ACS Catal.*, 2015, **5**, 4586-4591.
5. J. L. DiMeglio, J. Rosenthal, *J. Am. Chem. Soc.* **2013**, *135*, 8798-8801.
6. J. He, K. E. Dettelbach, D. A. Salvatore, T. Li, C. P. Berlinguette, *Angew. Chem. Int. Ed.* **2017**, *56*, 6068-6072.
7. R. Kas, K. K. Hummadi, R. Kortlever, P. de Wit, A. Milbrat, M. W. Luiten-Olieman, N. E. Benes, M. T. Koper, G. Mul, *Nat. Commun.* **2016**, *7*, 10748.
8. M. Ma, B. J. Trzesniewski, J. Xie, W. A. Smith, *Angew. Chem. Int. Ed.* **2016**, *55*, 9748-9752.
9. Y. Sun, J. Xu, X. Li, W. Liu, Z. Ju, T. Yao, C. Wang, H. Ju, J. Zhu, S. Wei, Y. Xie, *Angew. Chem. Int. Ed.* **2017**, *56*, 9121-9125.
10. S. Guo, S. Zhao, X. Wu, H. Li, Y. Zhou, C. Zhu, N. Yang, X. Jiang, J. Gao, L. Bai, Y. Liu, Y. Lifshitz, S. T. Lee, Z. Kang, *Nat. Commun.* **2017**, *8*, 1828.